

Generation of Coherent Phonons via a Cavity Enhanced Photonic Lambda Scheme

J. Bourhill,^{1,2} N. C. Carvalho,³ M. Goryachev,¹ Serge Galliou,⁴ and M.E. Tobar^{1,*}

¹ARC Centre of Excellence for Engineered Quantum Systems,
Department of Physics, University of Western Australia,
35 Stirling Highway, Crawley WA 6009, Australia

²IMT Atlantique and Lab-STICC (UMR 6285), CNRS,
Technopole Brest-Iroise, CS 83818, 29238 Brest Cedex 3, France

³Applied Physics Department and Photonics Research Center, University of Campinas, Campinas, SP, Brazil

⁴Department of Time and Frequency, FEMTO-ST Institute,
ENSMM, 26 Chemin de l'Épitaphe, 25000, Besançon, France

(Dated: December 22, 2024)

We demonstrate the generation of coherent phonons in a quartz Bulk Acoustic Wave (BAW) resonator through the photoelastic properties of the crystal, via the coupling to a microwave cavity enhanced by a photonic lambda scheme. This is achieved by imbedding a single crystal BAW resonator between the post and the adjacent wall of a microwave reentrant cavity resonator. This 3D photonic lumped LC resonator at the same time acts as the electrodes of a BAW phonon resonator, and allows the direct readout of coherent phonons via the linear piezoelectric response of the quartz. A microwave pump, ω_p , is tuned to the cavity resonance ω_0 , while a probe frequency, ω_{probe} , is detuned and varied around the red and blue detuned values with respect to the BAW phonon frequency, Ω_m . The pump and probe power dependence of the generated phonons unequivocally determines the process to be electrostrictive, with the phonons produced at the difference frequency between pump and probe, with no back action effects involved. Thus, the phonons are created without threshold and can be considered analogous to a Coherent Population Trapped (CPT) maser scheme.

One of the major hurdles to engineer quantum systems for applications such as sensing and scalable quantum computing is decoherence – the computational advantages of entanglement are lost if one's quantum state collapses too quickly. One main pathway of decoherence is the energy lost to the environment. Therefore, investigation into quantum hybrid systems that facilitate the transfer of energy from one form to another, an important protocol for quantum infrastructure, commonly look to utilise high quality factor resonators. As far as mechanical systems go, macroscopic single-crystal quartz bulk acoustic wave (BAW) resonators have demonstrated the largest $Q \times f$ products experimentally producible [1–5]. These crystals are specifically engineered with a convex curvature that traps phonons in the centre of the resonator, drastically reducing contact losses at its peripheries. Given the piezoelectric nature of quartz, coupling to the acoustic modes is straight forward and can be achieved with an RF source and two electrodes placed on either side of the crystal. Typically these electrodes are placed as close as possible to the crystal to achieve high electromechanical coupling, without touching, to preserve high mechanical Q -factors. Given their macroscopic size (weighing on the order of grams) and their excellent frequency stability, these devices have been proposed for use in tests of fundamental physics such as tests of Lorentz invariance [6, 7], quantum gravity [8], high frequency gravity wave detectors [9] and the search for scalar dark matter [10].

Only recently has optomechanical coupling to GHz mechanical modes in such crystals been achieved using two counter-propagating lasers [4, 5]. The afore-

mentioned work represents a new form of optomechanical system, and successfully interacts with the quartz mechanical modes without the use of piezoelectricity. Whilst piezoelectricity allows strong electromechanical coupling between photons and acoustic phonons, it is extremely valuable to explore coupling between different frequency ranges of these two interacting energy forms in order to improve the versatility and bandwidth of the quartz BAW as a potential quantum hybrid system. Here, we demonstrate coupling between a microwave resonant cavity and high quality factor quartz BAW resonant modes at MHz frequencies. This demonstration was achieved in two ways, firstly through the generation of mechanical sidebands on the microwave carrier when both phonon and photon modes are driven simultaneously, and secondly by exciting the acoustic mode (monitored via piezoelectricity) using two microwave tones, offset by the mechanical frequency. The latter is inherently a nonlinear effect given two GHz frequency tones produce a MHz frequency acoustic excitation, hence excitation via photoelasticity over piezoelectricity, with the later a linear phenomenon.

It was shown that there is no input power threshold for generation of phonons in the two tone setup, analogous to Coherent Population Trapped (CPT) masing [11–13], which operates on a similar principle, where the two photon tones excite an atomic transition without population inversion. Our analogous CPT phonon maser has important implications for transduction, allowing transduction of small photonic signals into mechanical frequencies.

The quartz BAW under study in this experiment was very similar to those used in [1]: a state of the art SC-

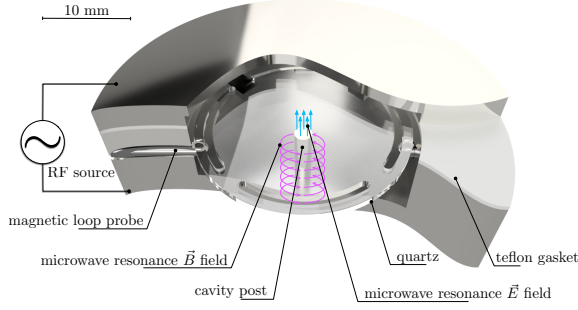


FIG. 1: Cut-away diagram of the device under test. The teflon gasket electrically isolates the top of the cavity from the bottom, allowing an RF source to piezoelectrically excite mechanical modes in the quartz.

cut (Stress Compensated) [14] quartz single crystal utilising BVA technology [15]. The resonator was ultrasonically machined into a planoconvex shape [16]; bulging on one side in its centre. A periphery supporting ring was also machined out of the single quartz crystal, which provides a location to hold the crystal in place. The BAW had a diameter of $d = 24.0$ mm, central thickness of $t = 1.00$ mm, and radius of curvature of the convex side of $R = 300$ mm. Three types of acoustic modes exist; longitudinal modes, fast shear modes, and slow shear modes, or A, B and C-modes, respectively; a result of the anisotropy of quartz. BVA resonators are constructed with “non-contacting” electrodes placed on either side of the crystal, allowing efficient electromechanical coupling through the quartz’s piezoelectricity. These electrodes will only detect a voltage difference across the crystal for an odd harmonic of the A, B or C modes; requiring opposite signed signals at either end of the crystal. Similarly, only odd harmonics can be excited by applying an RF voltage difference to the electrodes. The 3rd harmonic of the A, B and C modes for the given crystal at 4 K are located at 9.415,143 MHz, 5.500,049 MHz, and 4.996,171 MHz, respectively. The quality factors of these modes improve under vacuum and cryogenic conditions, capable of approaching $\sim 10^{10}$ [3].

The conducting surfaces of the electrodes potentially interfere with any microwave modes in a cavity QED-like experiment, so the mechanical resonator investigated here does not have any electrodes included. Instead, the top half and bottom half of the microwave cavity were insulated from each other by a teflon layer, allowing electromechanical coupling to the quartz crystal across the two halves of the cavity, which essentially allowed the cavity to also be implemented as electrodes (see Fig.1).

The microwave cavity takes the form of a re-entrant, or Klystron cavity [17]: an empty cylindrical space with a conducting post in the centre, which extends from one end-face towards the other, stopping short so as to form a gap between the top of the post and the lid of the cavity. The resonant microwave frequency re-entrant mode

is characterised by majority of electric field confined in this gap and the magnetic field circling around the post as shown in Fig.1, and thus the metallic rod forms a 3D lumped element LC resonator. The re-entrant cavity had a resonant frequency of 4.095 GHz. Microwaves were coupled into and out of the re-entrant cavity via co-axial cables, which were terminated by loops inside the cavity, hence producing an oscillating electromagnetic field. One of the main loss mechanisms at cryogenic temperatures is the surface resistance of the cavity walls. To minimise this, the cavity is constructed from pure Niobium, which becomes superconducting at ~ 9 K. However, the teflon gasket separating the two halves of the cavity resulted in some losses via leakage, limiting the microwave resonance’s Q -factor to about ~ 2000 at 4 K.

The quartz BAW resonator is placed within the gap between the re-entrant cavity’s post and lid – such that its centre overlaps with the location of highest microwave electric field concentration. This is because the centre of the crystal is the location of its mechanical modes, and a high degree of overlap between the mechanical and microwave modes will result in a larger photoelastic coupling. Recently a similar type of 3D cavity structure was used for transduction from microwave to optical frequencies[18]. The crystal was supported via three rigid blocks attached to the inside wall of the cavity upon which the peripheral support ring of the BAW makes contact. Due to the photoelastic effect, mechanical strain of the quartz results in a periodic modulation of the dielectric permittivity over the crystal volume. This modulation changes the nature of the media through which the resonant re-entrant mode’s electric field is oscillating. This results in a frequency shift of the microwave mode and hence a form of optomechanical coupling. Via the inverse process; electrostriction (or photoelastic response), an applied electric field induces strain within the crystal due to a slight displacement of ions.

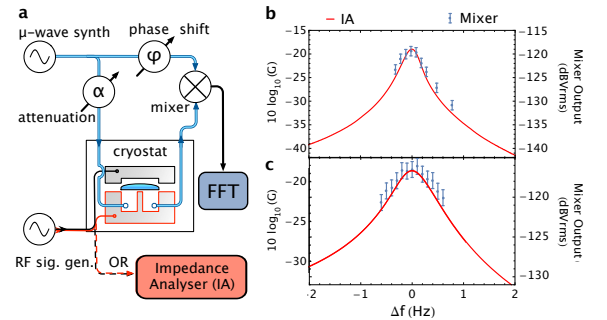


FIG. 2: **a** Simplified experimental phase bridge setup for observing mechanical sidebands on the microwave carrier and calibrating the electromechanical coupling. **b** (**c**) Mixer output compared to impedance analyser measurement of 4.996 MHz (9.415 MHz) mode. Error bars on the mixer readings are determined from repeat measurements for a given detuning.

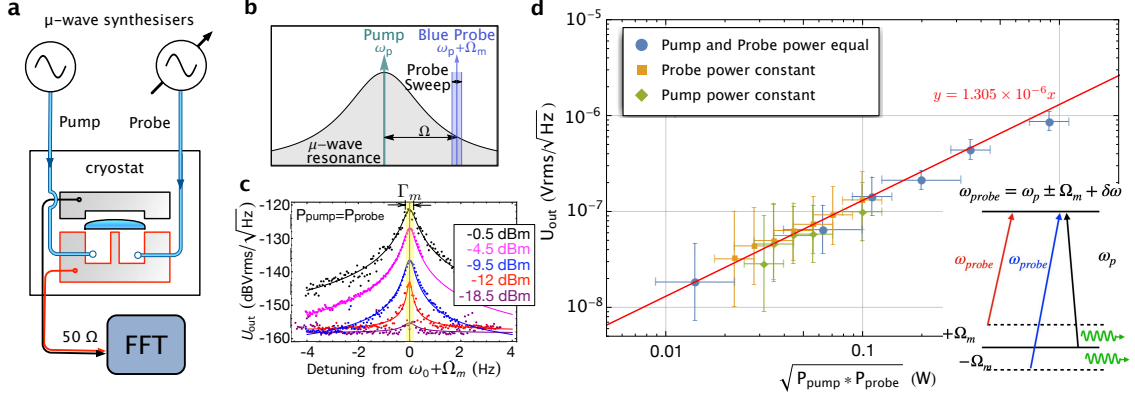


FIG. 3: **a** Simplified “Lambda-scheme” or “two-tone” experimental setup to generate coherent phonons at the difference frequency of the pump (ω_p) and probe frequency (ω_{probe}). **b** Spectral representation of “two-tone” experiment for the blue-detuned case. **c** Electrode output as a function of probe detuning from $(\omega_p + \Omega_m)/2\pi$ for different pump and probe powers ($P_{pump} = P_{probe}$, values given in the legend) for the $\Omega_m = 4.996$ MHz acoustic mode. Each point represents a single experiment that either generates a coherent phonon, or if too weak, measures the back ground noise floor. **d** Electrode output as a function of $\sqrt{P_{pump} \times P_{probe}}$ when $\delta\omega = 0$ (or zero detuning), demonstrating a linear relationship that intercepts $\{0, 0\}$, suggesting no threshold power in the process. Horizontal errors are determined from the uncertainty in input and output line attenuations in the cryostat and vertical uncertainties from repeat measurements for given input powers. The equivalent energy diagram similar to a CPT maser is shown as an inset.

The optomechanical coupling was determined by exciting the quartz mechanical modes piezoelectrically, and measuring the effect on the resonant microwave mode using a “phase-bridge” setup. To do this, a setup like that in figure 2 (a) was used. A microwave synthesiser continuously pumps the re-entrant cavity mode at ~ 4.095 GHz, whilst an RF signal generator applies a MHz signal across the cavity lid and base. The transmitted microwave signal is then mixed down against the input signal from the synthesiser, which is phase shifted such that the mixer will output a voltage proportional to any phase shift produced in the resonator, which is manifested as a frequency shift in the resonator’s arm of the bridge. By observing the output spectra of the mixer on an Agilent 89410A Vector Signal Analyser (FFT), one can measure the strength of modulation on the resonant microwave mode caused by the mechanical motion of the quartz. By applying a continuous wave RF voltage across the microwave cavity this can be done in the static regime - measuring the mixer output at and around mechanical resonant frequencies. The results of this experiment, sweeping the signal generator over the 4.996 MHz and 9.415 MHz modes are shown in Fig. 2(b) and (c), respectively by the blue points. These measurements were taken with synthesiser power at 15 dBm, attenuation to the cavity $\alpha = 18$ dBm, and a 10 mV amplitude signal applied by the RF signal generator around the mechanical resonance frequency. The conversion efficiency of the phase-bridge setup (the voltage output by the mixer given some frequency shift in the resonator arm) is measured using an artificial modulation signal to be $du/df = 11.7 \mu\text{V/kHz}$.

The acoustic resonances of the quartz were also directly measured by an impedance analyser connected across the microwave cavity. From the measurements of impedance and phase, one can determine the conductance, G across the “electrodes”, which is plotted in red for the 4.996 MHz and 9.415 MHz modes in Fig.2(b) and (c), respectively. We see that the static measurements of the phase bridge mixer output match the measurements of G within experimental error, given some coefficient of mixer conversion efficiency. This demonstrates that the modulation of the microwave resonant mode measured by the phase bridge was a result of the mechanical excitation. These measurements also allow an accurate way to determine Q factors; 1.607×10^7 for the 4.996 MHz mode and 1.264×10^7 for the 9.415 MHz mode, and the L , C and R values for the equivalent electrical circuit of the mechanical resonance. These measurements also allowed the determination of the displacement of the quartz crystal when the aforementioned 10 mV signal was applied, and hence the single-photon optomechanical coupling rate, g_0 . The value g_0 represents the frequency shift of the electromagnetic mode caused by the displacement of the mechanical system when a single photon enters the electromagnetic system.

The charge q and displacement x in a piezoelectrical system are related in a linear fashion by an electromechanical coupling constant k [9]:

$$q = kx, \quad (1)$$

where

$$k^2 = \frac{\Omega_m M_{\text{eff}}}{Q R}. \quad (2)$$

Here, M_{eff} is the effective mass of the resonance, $\Omega_m/2\pi$ the resonant frequency, and R its effective resistance. For $\Omega_m/2\pi = 4.996$ MHz, an rms charge is determined from the applied $V_{\text{rms}} = 10/\sqrt{2}$ mV and the equivalent resistance $R = 78.5 \Omega$. $M_{\text{eff}} = 1.13 \times 10^{-5}$ kg is determined from finite element modelling [19]. This nets an rms displacement of $x = 5.52$ nm. The simple relationship

$$\frac{\delta u}{\delta x} = \frac{du}{df} \frac{df}{dx} \quad (3)$$

will allow us to relate the calculated displacement $\delta x = x$ to the output voltage of the mixer δu from the aforementioned frequency sensitivity of the phase bridge du/df and the dependence of the electromagnetic frequency on displacement $df/dx = g_0/x_{\text{zpf}}$, where $x_{\text{zpf}} = \sqrt{2/\hbar\Omega_m M_{\text{eff}}}$ is the so-called zero-point fluctuation of the mechanical resonance. Substituting in all relevant numerical values nets a single-photon optomechanical coupling rate of $g_0 = 8.43$ nHz, which is in excellent agreement with simulated results of the photoelastic coupling rate in this system [19].

The second technique used to excite the mechanical modes involved two microwave tones in a Brillouin-like setup [4]. The two signals were input to the microwave cavity via loop probes, and the spectra of the potential difference across the cavity was measured on a FFT spectrum analyser as shown in figure 3(a). The output voltage measured in this way was therefore directly proportional to the displacement of the piezoelectric quartz.

The FFT window was centred at the acoustic resonant frequency with a 10 Hz span; aiming to detect the voltage spectra produced by the mechanical motion of the piezoelectric quartz. One microwave signal; the pump, was tuned on resonance $\omega_p = \omega_0$, whilst the other; the probe, was detuned by some amount. The probe microwave source was swept from $f_1 = (\omega_p - \Omega_m)/2\pi - 5$ to $f_2 = (\omega_p - \Omega_m)/2\pi + 5$ in the red detuned case, and $f_1 = (\omega_p + \Omega_m)/2\pi - 5$ to $f_2 = (\omega_p + \Omega_m)/2\pi + 5$ in the blue detuned case. This scheme is demonstrated in figure 3(b) for the blue-detuned case. Results of the red-detuned case are identical.

The output voltage produced by the quartz crystal is plotted in fig 3c as the probe synthesiser is detuned from $\omega_0 + \Omega_m$. Mechanical motion of the quartz is generated through the nonlinear mixing of the two microwave input signals, a result of electrostriction. Electrostriction (or photoelasticity) is a quadratic phenomenon that relates strain to the square of electric polarisation according to:

$$S_{ij} = Q_{ijkl}\chi^2\epsilon_0^2 E_k E_l, \quad (4)$$

where S_{ij} is the second-order strain tensor, Q_{ijkl} the four rank electrostriction coefficient, χ the electrical susceptibility (can be simplified to a scalar) and E_k, E_l electric fields. The quadratic nature of the electrostriction generates a double frequency and difference frequency term.

When the difference frequency is equal to a mechanical resonant frequency of the quartz crystal, it will be resonantly enhanced. Given the piezoelectric nature of the quartz, this will generate an electric field at the same difference frequency, and hence a voltage across the “electrodes”; i.e. the top and the bottom of the cavity.

The strain produced by electrostriction acts as a driving term in the piezoelectric equations of motion [20]. A full theoretical derivation of this process is given in the supplementary materials in which it is demonstrated that the voltage across the top and bottom of the cavity $U_{\text{out}} \propto E_{\text{pump}} E_{\text{probe}} \propto \sqrt{P_{\text{pump}} P_{\text{probe}}}$. The dependence of U_{out} on the pump and probe powers is plotted in figure 3d, demonstrating this proportionality.

Given the microwave mode being used is a standing wave, the typical phase matching conditions of a Brillouin scheme are lifted. Instead, all that is necessary for the generation of mechanical phonons is conservation of energy between the two microwave fields and the acoustic mode. This scheme is analogous to CPT masing [11–13], in which two detuned optical pumps generate a microwave signal at the frequency of a hyperfine splitting, detected directly through stimulated emission in a cavity. Here, generated phonons are directly detected through the electrical readout on either side of the piezoelectric quartz. Exactly like CPT masing, the observed excitation demonstrates no “threshold” for onset, as shown by Fig.3d. The allowable bandwidth of the excited coherent phonons (figure 3c) increases as a function of applied power, demonstrated in figure 4.

In conclusion we have demonstrated a way to calibrate an optomechanical system coupled through a nonlinear electrostrictive coupling. By implementing a two-photon lambda excitation coherent phonons were gen-

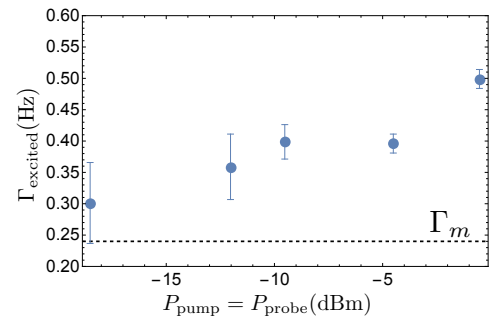


FIG. 4: 3dB bandwidth of the phonon generation process Γ_{phonon} as a function of applied microwave power. The bandwidth of the possible phonon generation is centred around the BAW acoustic frequency and is larger than the intrinsic bandwidth $\Gamma_m = \Omega_m/Q_m$ of the BAW acoustic mode. The bandwidth increases as a function of power as shown, and for the range of powers we applied it was more than a factor of two greater than the intrinsic linewidth. Error bars are estimated from fitting Lorentzian functions to the line-shapes of figure 3c.

erated, with a bandwidth of generation greater than the acoustic linewidth. This technique is analogous to a CPT maser, and gives a way to generate coherent phonons with no power threshold.

The data that support the findings of this study are available from the corresponding author upon reasonable request.

This work was supported by Australian Research Council grant number CE170100009 and a UWA Research Collaboration Award with IMT-Atlantique.

* michael.tobar@uwa.edu.au

- [1] M. Goryachev, D. L. Creedon, E. N. Ivanov, S. Galliou, R. Bourquin, and M. E. Tobar, Applied Physics Letters **100**, 243504 (2012), <https://doi.org/10.1063/1.4729292>.
- [2] M. Goryachev, D. L. Creedon, S. Galliou, and M. E. Tobar, Phys. Rev. Lett. **111**, 085502 (2013).
- [3] S. Galliou, M. Goryachev, R. Bourquin, P. Abbé, J. P. Aubry, and M. E. Tobar, Scientific Reports **3**, 2132 (2013).
- [4] W. H. Renninger, P. Kharel, R. O. Behunin, and P. T. Rakich, Nature Physics (2018), 10.1038/s41567-018-0090-3.
- [5] P. Kharel, G. I. Harris, E. A. Kittlaus, W. H. Renninger, N. T. Otterstrom, J. G. E. Harris, and P. T. Rakich, Science Advances **5** (2019), 10.1126/sciadv.aav0582.
- [6] M. Goryachev, Z. Kuang, E. N. Ivanov, P. Haslinger, H. Müller, and M. E. Tobar, IEEE Transactions on Ultrasonics, Ferroelectrics, and Frequency Control **65**, 991 (2018).
- [7] A. Lo, P. Haslinger, E. Mizrachi, L. Anderegg, H. Müller, M. Hohensee, M. Goryachev, and M. E. Tobar, Physical Review X **6**, 011018 (2016).
- [8] P. A. Bushev, J. Bourhill, M. Goryachev, N. Kukharchyk, E. Ivanov, S. Galliou, M. E. Tobar, and S. Danilishin, Phys. Rev. D **100**, 066020 (2019).
- [9] M. Goryachev and M. E. Tobar, Phys. Rev. D **90**, 102005 (2014).
- [10] A. Arvanitaki, S. Dimopoulos, and K. V. Tilburg, Physical Review Letters **116** (2016).
- [11] A. Godone, F. Levi, S. Micalizio, and J. Vanier, Phys. Rev. A **62**, 053402 (2000).
- [12] J. Vanier, Applied Physics B **81**, 421 (2005).
- [13] A. Godone, F. Levi, S. Micalizio, and C. Calosso, Phys. Rev. A **70**, 012508 (2004).
- [14] E. EerNisse, in *29th Annual Symposium on Frequency Control* (Electronic Industries Association, 1975) pp. 1–4.
- [15] R. Besson, in *31st Annual Symposium on Frequency Control* (Electronic Industries Association, 1977) pp. 147–152.
- [16] D. Stevens and H. Tiersten, J. Acous. Soc. Am. **79** (1986).
- [17] J.-M. L. Floch, Y. Fan, M. Aubourg, D. Cros, N. C. Carvalho, Q. Shan, J. Bourhill, E. N. Ivanov, G. Humbert, V. Madrangeas, and M. E. Tobar, Review of Scientific Instruments **84**, 125114 (2013), <https://doi.org/10.1063/1.4848935>.
- [18] H. Ramp, T. J. Clark, B. D. Hauer, C. Doolin, K. C. Balram, K. Srinivasan, and J. P. Davis, Applied Physics Letters **116**, 174005 (2020), <https://doi.org/10.1063/5.0002160>.
- [19] N. C. Carvalho, J. Bourhill, M. Goryachev, S. Galliou, and M. E. Tobar, Applied Physics Letters **115**, 211102 (2019), <https://doi.org/10.1063/1.5127997>.
- [20] D. S. Stevens and H. F. Tiersten, The Journal of the Acoustical Society of America **79**, 1811 (1986), <https://doi.org/10.1121/1.393190>.

SUPPLEMENTARY MATERIAL

Output voltage from two applied microwave sources

We drive the microwave cavity with two tones, E^{pump} at frequency ω_0 and E^{probe} at frequency $\omega_0 + \Delta$, where ω_0 is the microwave resonant frequency of the cavity. Given the re-entrant cavity architecture, the electric field exists between the top of the post and the roof of the cavity and can therefore be approximated as the electric field inside a capacitor; i.e. in the cavity's z -direction and uniform throughout. Therefore we can write the electric fields between the top of the post and the roof of the cavity as:

$$E^{\text{pump}}(t) = E_0^{(1)}(e^{i\omega_0 t} + e^{-i\omega_0 t})\hat{\mathbf{e}}_z \text{ and} \\ E^{\text{probe}}(t) = E_0^{(2)}(e^{i(\omega_0 + \Delta)t} + e^{-i(\omega_0 + \Delta)t})\hat{\mathbf{e}}_z, \quad (5)$$

where E_0^i is the electric field amplitude and ϕ and θ represent the phase of both signals.

The two electric fields across the quartz crystal will interact via electrostriction; a quadratic phenomenon that relates strain to the square of electric polarisation P , according to:

$$S_{ij} = Q_{ijkl}P_kP_l = Q_{ijkl}\chi^2\epsilon_0^2E_kE_l = M_{ijkl}E_kE_l, \quad (6)$$

where S_{ij} is the second-order strain tensor, Q_{ijkl} the four rank electrostriction tensor coefficient, $\chi = \epsilon_r - 1$ the electrical susceptibility and E_k, E_l electric fields. Substituting $E^{(1)}$ and $E^{(2)}$ into 6 gives:

$$S_{ij} = Q_{ijkl}\chi^2\epsilon_0^2E_0^{(1)}E_0^{(2)}(e^{i(2\omega_0 + \Delta)t} + e^{i\Delta t} + c.c.)\hat{\mathbf{e}}_z\hat{\mathbf{e}}_z \\ = K_{ijkl}E_0^{(1)}E_0^{(2)}[(e^{i(2\omega_0 + \Delta)t} + e^{i\Delta t} + c.c.)]\hat{\mathbf{e}}_z\hat{\mathbf{e}}_z \quad (7)$$

Given the two applied E -fields are forced into the z -direction (X_3 in figure 5) by the cavity, it follows that strain components S_{ij} will be determined by the electrostriction tensor components Q_{ij33} (modified in this case to K_{ij33}). If $\Delta = \Omega_m^i$ (i.e. $\Delta \ll \omega_0$), the frequency of a resonant mechanical BAW mode in the quartz crystal, the low frequency component in equation 7 will generate strain at the frequency Ω_m^i which will be resonantly enhanced, and hence we can ignore the higher frequency term, which will not be seen by the mechanical system. This strain term will appear as an additional term in the standard piezoelectric differential equation of motion [20]:

$$T_{ij} = c_{ijkl}\frac{\partial u_k}{\partial x_l} + e_{kij}\frac{\partial \varphi}{\partial x_k}, \\ D_i = e_{ikl}\frac{\partial u_k}{\partial x_l} - \epsilon_{ij}\frac{\partial \varphi}{\partial x_j}, \\ \frac{\partial T_{ij}}{\partial x_i} = \rho\ddot{u}_j, \quad \frac{\partial D_i}{\partial x_i} = 0, \quad (8)$$

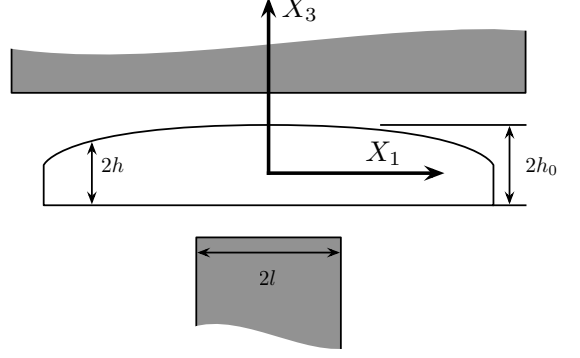


FIG. 5: Schematic diagram showing a cross section of the plano-convex quartz resonator inside the re-entrant cavity

where T_{ij} , u_j , and D_i are the components of stress, mechanical displacement, and electric displacement, respectively; ρ and φ are the mass density and electric potential, respectively; and c_{ijkl} , e_{ikl} and ϵ_{ij} are the elastic, piezoelectric, and dielectric constants, respectively.

Given we deal with a plano-convex crystal architecture (see fig. 5) and are interested in only the third overtone of the pure shear mode (with resonant frequency $\Omega_m^{(300)}$) the equation of motion for displacement becomes [20] (setting the tunable $\Delta = \omega$):

$$M_3\frac{\partial^2 u_1}{\partial x_1^2} + P_3\frac{\partial^2 u_1}{\partial x_2^2} - \frac{3^2\pi^2\bar{c}^{(1)}}{4h_0^2}\left(1 + \frac{x_1^2 + x_2^2}{2Rh_0}\right)u_1 \\ + \rho\omega^2 u_1 = -\rho\omega^2 K_{1133}E_0^{(1)}E_0^{(2)}e^{i\omega t}, \quad (9)$$

where $u_1 = u(x_1, x_2)e^{i\omega t}$ is the component of mechanical displacement in the X_1 direction; M_n , Q_n and P_n are constants formulated from various elastic tensor and dimensional values [20]; h_0 and R are the height of the crystal at its centre and its radius of curvature, respectively; and $\bar{c}^{(1)} = \rho\omega^2/\eta_1^2$, where $\eta_1 = \omega/v_1$, where v_1 is the speed of the acoustic wave in the X_1 direction.

Equation 9 will have solutions of the form:

$$u_1 = H^{300}u_{300}\sin\frac{3\pi x_3}{2h}e^{i\omega t}, \\ \varphi = \frac{e_{36}}{\epsilon_{33}}H^{300}u_{300}\left(\sin\frac{3\pi x_3}{2h} + \frac{x_3}{h}\right)e^{i\omega t}, \\ \text{where } H^{300} = \frac{-K_{1133}E_0^{(1)}E_0^{(2)}\sqrt{\alpha_3}\sqrt{\beta_3}4F_{130}F_{330}}{1 - \Omega_m^2/\omega^2}, \\ F_{130} = \int_0^{l_1} e^{-\alpha_3(x_1^2/2)}dx_1, \quad F_{330} = \int_0^{l_2} e^{-\beta_3(x_2^2/2)}dx_2 \\ u_{300} = e^{-\alpha_3(x_1^2/2)}e^{-\beta_3(x_2^2/2)}, \\ \alpha_n^2 = \frac{n^2\pi^2\bar{c}^{(1)}}{8Rh_0^3M_n}, \quad \beta_n^2 = \frac{n^2\pi^2\bar{c}^{(1)}}{8Rh_0^3P_n}, \quad (10)$$

and, as usual, Ω_m is replaced by

$$\hat{\Omega}_m = \Omega_m + i\Omega_m/2Q, \quad (11)$$

in which Q is the unloaded quality factor of the resonant mode. From equation 8, and assuming some scalar potential φ exists from the resulting electric field where quantities are varying at ω , and various simplifications [20] we can state that

$$D_3 = e_{36} \frac{\partial u_1}{\partial x_3} - \epsilon_{33} \frac{\partial \varphi}{\partial x_3} = \frac{-e_{36} H^{300} u_{300}}{h_0} e^{i\omega t}, \quad (12)$$

from which the current generated by the crystal's motion can be obtained by integrating over the crystal area:

$$I = - \int_{A_e} \dot{D}_3 dx_1 dx_2 = \frac{i\omega e_{36} H^{300}}{h_0} \int_{A_e} u_{300} dx_1 dx_2, \quad (13)$$

where A_e is the area of the “electrodes”, and we are able to remove all terms independent of x_1 and x_2 from the integration, which assumes the electric fields E_0^i are constant over the area of the crystal.

The current generated by the crystal between the electrodes is received at the 50Ω terminal of the FFT device as a voltage U_{out} . We can see from the from of equation 13 that the amplitude of this voltage will be proportional to H_{300} and hence $E_0^{(1)} E_0^{(2)}$ when $\omega = \Omega_m$ i.e. the detuning $\Delta = \Omega_m$.

Given we are assuming these fields are approximately those of a parallel plate capacitor we can relate the amplitude of the fields to the input power of the driving signals by considering the entire microwave cavity system as a lumped parallel LCR circuit and therefore the voltage drop across the capacitor to its reactance, $X_c(\omega)$ and the input powers, P^i :

$$E_0^{(1)} = \frac{\sqrt{X_c(\omega_0)P^{(1)}}}{d}, \text{ and } E_0^{(2)} = \frac{\sqrt{X_c(\omega_0 + \Delta)P^{(2)}}}{d}, \quad (14)$$

where d is the distance between the top of the post and the roof.

Therefore, we can state that the voltage U_{out} read from the FFT will have the proportionality:

$$U_{\text{out}} \propto \sqrt{P^{(1)}P^{(2)}} \quad (15)$$